Ceramics-Silikáty 69 (2), 254-262 (2025)
www.ceramics-silikaty.cz doi: 10.13168/cs.2025.0010

PROPERTIES OF A YOUNG FLY ASH BASED GEOPOLYMER CONCRETE RELATED TO THE MODULUS OF SODIUM WATER GLASS

DAIDAI LIN*, #YINGKUN XUE**, WENRUI XU**, YONGLIANG HAN***

*College of Economy and Finance, Shaanxi Technical College of Finance & Economics, Xianyang, 712099, PR China
**College of Civil Engineering, Xi'an University of Architecture and Technology, Xi'an, 710055, PR China
***CCTEG Xi'an Research Institute (Group) Co., Ltd., Xi'an, 710077, PR China

#E-mail: 1210800816@qq.com

Submitted November 13, 2024, accepted February 19, 2025

Keywords: Fly ash based geopolymer concrete, Sodium water glass, Modulus, Alkali activation characteristics, Microstructure

This study systematically investigates the effects of sodium water glass with a different modulus (1.0, 1.3, 1.6) on the early age strength, alkali activation characteristics, and microstructure of fly ash based geopolymer concrete (FABGC). The results show that as the modulus of sodium water glass increases, the compressive strength of FABGC first increases and then decreases, and the total heat release of the alkali activated system gradually decreases. Although the modulus of sodium water glass has no significant effect on the phase types of FABGC, it has a significant impact on the carbonate content in FABGC. The cumulative pore volume of FABGC first decreases and then increases with the increase of modulus of sodium water glass, and the modulus of sodium water glass has a significant impact on the different pore ratios. In summary, when the modulus of sodium water glass is 1.3, FABGC has a relatively dense microstructure, and its early-age performance is excellent.

INTRODUCTION

As a new type of green building material, geopolymer concrete has 20-50 % lower carbon emissions than ordinary concrete in the manufacturing process [1]. The most representative geopolymer precursor cementitious materials are metakaolin, fly ash (FA) and slag (S) [2-4]. Compared to geopolymer concrete made from metakaolin, the production process of fly ash based geopolymer concrete (FABGC) is relatively simple [5]. Compared to alkali-activated slag concrete, FABGC has stronger high temperature resistance and lower deformation due to the shrinkage deformation and creep [5-7]. In addition, the cost of producing FABGC is lower, which favours its dissemination and application.

The type and modulus of the alkaline activator have a significant impact on the performance of FABGC. Currently, the most commonly used alkaline activators in the production of FABGC are NaOH, $Na_2O{\cdot}nSiO_2$ (where n represents the modulus), and KOH [8]. When compared to other alkaline activators, the sodium water glass solution formed by mixing NaOH with $Na_2O{\cdot}nSiO_2$ exhibits a superior excitation effect. OH^- facilitates the dissolution of FA particles and assists in forming silicon-oxygen tetrahedron and aluminium-oxide tetrahedron [9, 10]. The presence of soluble silicate speeds up alkali-activation reactions and promotes the formation of a com-pact gel [11-13]. However, excess OH^- in the sodium water glass solution hinders the polymerisation process by causing rapid precipitation of aluminosilicate [14]. In addition, when the silicate is excessive, the strength of FABGC develops slowly, so the modulus of sodium water glass has an important influence on the performance of FABGC [15, 16]. Cao et al. [17] investigated the impact of the sodium water glass modulus (0.6-1.4) on the mechanical properties of alkali-activated FA/S geopolymer concrete. Their findings revealed that as the sodium water glass modulus increased, the strength of alkali-activated FA/S geopolymer concrete initially increased and then declined. The highest strength of the geopolymer concrete was observed at a modulus of 1.0. Cho et al. [18] found that when the modulus of sodium water glass increased from 0.8 to 2.0, the compressive strength of FABGC first increased and then decreased. When the modulus of sodium water glass is 1.4, the compressive strength of FABGC reaches its maximum value at 28-d. Huseien et al. [19] demonstrated that as the modulus of sodium water glass increases, the production of calcium oxide within the alkali-activated FA/S geopolymer mortar is significantly increased, and the formation of C-S-H gels is also increased. However, surplus calcium oxide reacts with CO_2 at an excessively

high modulus to produce calcite. In addition, as the modulus of sodium water glass increases, the number of unreacted FA and S particles in the alkali-activated FA/S geopolymer mortar matrix decreases, resulting in a denser geopolymer matrix. A higher S content accelerates the alkali-activation reaction, leading to the formation of C-S-H or C-A-S-H gels enhancing the strength of geopolymer mortar [19-21]. In summary, the modulus of sodium water glass significantly affects the mechanical properties and microstructure of FABGC. However, the current research focuses on this influence and rarely reveals the relevant mechanism from the micro-structure evolution level.

This paper systematically studied the effects of the sodium water glass modulus on the early age compressive strength, alkali activation characteristics, phase composition, pore structure, and microstructure of FABGC. The mechanism of the influence of the sodium water glass modulus on the mechanical properties of FABGC was revealed, which provides a theoretical basis for further optimising the performance of FABGC.

EXPERIMENTAL

Materials and mixture proportions

The cementitious materials consist of Class F FA and S95 grade S. FA has a 45 μm sieve residue of 7.5 % and a loss on ignition of 2.3 %. S has a 45 μm sieve residue of 7.4 % and a loss on ignition of 0.1 %. Refer to Table 1 for their chemical compositions. The alkaline activator is a sodium water glass solution formed by mixing NaOH with water glass. NaOH is a white, flaky solid with a purity of 98 % or higher. The modulus of water glass is 3.2, with Baumé degree of 40. It contains 26.5 % SiO_2, 8.5 % Na_2O, and 60 % water. The fine stuff is medium sand (SA), with a maximum aggregate size of 4.75 mm, a fineness modulus of 2.7, a bulk density of 1500 kg·m^{-3}, and an apparent density of 2640 kg·m^{-3}. The coarse aggregate comprises limestone crushed stone (LS) with a gradation of 5-25 mm, a crushing index of 8.3 %, a bulk density of 1540 kg·m^{-3}, and an apparent density of 2700 kg·m^{-3}. The mixing water used is laboratory tap water (W).

Due to the low calcium content of the FA, adding an appropriate amount of S can enhance the calcium content of the cementitious material, improving the FABGC performance. However, an excessive S addition can increase the FABGC's shrinkage characteristics. Generally, the optimal dosage of S is 15-30 % of the total amount of cementitious materials [22, 23]. Therefore, the dosage of S in this study is 20 %. The modulus of the sodium water glass significantly affects the alkali-activation reaction of FA/S. A lower modulus in the sodium water glass increases the alkalinity, improving the dissolution of FA particles and the alkali-activation reaction. However, an excessively low modulus leads to rapid depolymerisation and polymerisation reactions on the FA particle surface, forming a "passivation film". This film impedes the full reaction of silicon-aluminium materials, leading to the suboptimal development of FABGC strength. Prior studies [17, 18, 24] suggest that the optimal modulus for sodium water glass falls between 0.8 and 1.8. Therefore, this study establishes the sodium water glass modulus as 1.0, 1.3, and 1.6. The mixture proportions of FABGC are listed in Table 2.

Sample preparation

Before preparing the test sample, mix NaOH and water glass solution in the correct proportion to create sodium water glass solution, and let it stand for 24 hours. The FABGC mixture is blended in a single-horizontal-axis concrete mixer. First, pour the cementitious material and coarse and fine aggregates into the mixer, and dry mix for 90 seconds until fully mixed. Slowly add the sodium water glass solution and continue stirring for 270 s. Completing the mixing process, transfer the mixture into a test mould measuring 100 × 100 × 100 mm and compact it using a vibration table. The FABGC specimen was sealed, demoulded after standing at room temperature for 24 hours, wrapped in a thin film, and cured in an oven at 80 °C for 24 hours. Completing the high-temperature curing, remove the film and place the specimen under conditions of 20 ± 2 ℃ and 50 ± 5 % relative humidity for further curing. After reaching the specified age, the specimens should be removed for the mechanical property and microstructure testing.

Table 1. Chemical composition of the binder (%).

Material	SO_3	CaO	SiO_2	Al_2O_3	Fe_2O_3	MgO	Other
FA	2.16	4.76	50.26	31.14	4.16	4.12	3.40
S	1.64	34.0	34.50	17.70	1.03	6.01	5.12

Table 2. FABGC mixture proportions (kg·m^{-3}).

Number	FA	S	SA	LS	W	NaOH	Na_2SiO_3	Modulus of sodium water glass solution (Ms)
Ms-1.0	344	86	648.2	1316	85.9	29.24	97.50	1.0
Ms-1.3	344	86	648.2	1316	66.5	26.30	131.0	1.3
Ms-1.6	344	86	648.2	1316	52.0	24.80	155.8	1.6

Test method

Compressive strength

Test the compressive strength of FABGC at 3-d, 7-d, 14-d, and 28-d following the GB/T 50081-2002 standard for the test method of mechanical properties on ordinary concrete [25]. Utilise a uniform and continuous loading approach, aiming for a rate of 0.5-0.8 MPa·s^{-1}. For each mix proportion, three specimens are tested, and the average value is considered the compressive strength test result for that group.

Alkaline activation characteristics

The exothermic quantity and rate of the alkaline-activation reaction of FABGC were measured using a TAM Air eight-channel microcalorimeter over a temperature range of 5-90 °C. The constant temperature bath had an accuracy of ± 0.2 °C, with a detection limit of 4 μW and a precision of ± 20 μW. During specimen preparation, 3.2 g of FA and 0.8 g of S are used, and the amounts of NaOH, Na_2SiO_3, and water are calculated based on the mixture proportions, excluding aggregates. The alkali activation heat release and heat release rate of the FA/S system was then tested for 160 hours at 20 °C.

Phase composition

The phase composition of FABGC was analysed using X-ray diffraction (XRD). Fragments located about 5 mm from the specimen's surface were ground into a powder then dried in an oven at 50 °C for 24 hours. An EMPYREAN X-ray powder diffractometer produced by PANalytical in the Netherlands was used. It has a diffraction angle (2θ) range of 10 to 70° with a step size of 0.02°. Cu-Kα radiation and a graphite monochromator were used to record diffraction beams at different angles. The XRD test results were analysed by Jade software.

Pore structure

An AutoPore® IV9500 mercury intrusion porosimeter was used to analyse the pore structure of the FABGC. After curing the FABGC specimens for 3-d, 7-d, 14-d, and 28-d, they were crushed into small pieces. A mortar piece with a 3-5 mm diameter is chosen and soaked in an ethanol solution to halt the alkaline-activation reaction. Prior to conducting the pore structure test, remove the sample from the ethanol solution. Allow the ethanol to evaporate completely, then dry the sample in an oven at 55 ℃ [26]. After drying the sample to a constant weight, conduct the pore structure test.

Microscopic morphology

The microstructure of the FABGC specimens was analysed using a Gemini SEM 500 cold field emission scanning electron microscope (SEM-EDS). The voltage was 3.0 kV and magnification ranging from ×0.05 K to × 2000 K. Before the test, the specimen had a diameter of approximately 3-5 mm, a relatively flat surface, and no clear edges or corners. The sample was adhered to the red copper sample holder using a double-sided conductive adhesive, and sprayed gold in a vacuum. Finally, the pre-processed sample was placed into the instrument to observed the microstructure of the FABGC.

RESULTS AND DISCUSSION

Compressive strength

The trend of the FABGC compressive strength over time is shown in Figure 1. At the same age, Ms-1.0 and Ms-1.3 exhibit higher compressive strength than Ms-1.6. With the extension of the curing time, the compressive strength of both Ms-1.0 and Ms-1.3 consistently increases. However, after 7 d, the compressive strength of Ms-1.6 shows a slower growth rate, and its difference in compressive strength compared to the other two groups widens progressively. At 28 d, the compressive strength of Ms-1.0 and Ms-1.3 both exceeds 50 MPa, while that of Ms-1.6 is around 40 MPa. When the modulus is too high, the concentration of hydroxyl ions in the sodium water glass solution is low [27], the FA particles and S particles cannot be fully dissolved, and the production of N(C)-A-S-H and C-S-H gel decreases, resulting in the poor strength development of FABGC.

Alkaline activation characteristics

The exothermic rate curves of the alkali-activated reaction process in the alkali-activated FA/S composite system can be categorised into three groups [28], as illustrated in Figure 2. The exothermic curve of the

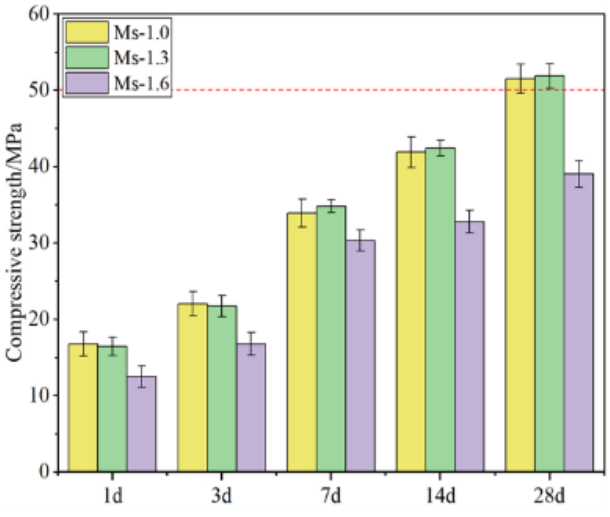

Figure 1. Compressive strength of the different FABGCs.

first type of alkali-activation reaction shows only one exothermic peak in the initial reaction stage without a clear division of reaction stages. The exothermic curve for the second type of alkali-activation reaction is similar to the third one, both divided into five stages: initial hydration stage, induction period, acceleration period, decay period, and extended period. However, the third type shows two exothermic peaks during the initial hydration stage, while the second has only one.

As depicted in Figure 3(a), the exothermic rate of the alkali-activated FA/S system reaches its peak within 0.2-0.5 hours. This is attributed to the rapid dissolution of the vitreous structure on the surface of the FA/S particles when they come into contact with the sodium water glass solution, leading to a noticeable "high and sharp" initial hydration peak within the first 0.5 hours [29]. Additionally, as the modulus of sodium water glass increases, the relative content of Na_2O in the sodium water glass solution decreases, leading to the reduced solubility of the FA and S particles and a longer time for the FA/S system to reach peak reaction rate. As the reaction time increases, the exothermic rate of the alkali-activation reaction in the FA/S system gradually decreases. In Ms-1.0, the FA/S system shows the highest exothermic rate between 50-160 hours. It is noteworthy that, in Ms-1.3, the FA/S system exhibits the greatest peak reaction rate. As illustrated by the cumulative heat release curve of the alkali-activation reaction in Figure 3(b), during the initial stage of the alkali-activation reaction (0-0.5 h), the cumulative heat release curves of the alkali-activated FA/S systems prepared with various sodium water glass moduli are essentially identical. However, after 50 hours, the total heat release of the FA/S systems with Ms-1.0 and Ms-1.3 are greater. In addition, the total heat release from the alkali activation of the alkali-activated FA/S system decreases as the sodium water glass modulus increases. This suggests that the alkali-activation reaction of the FA/S system was sufficient when the modulus of sodium water glass was low.

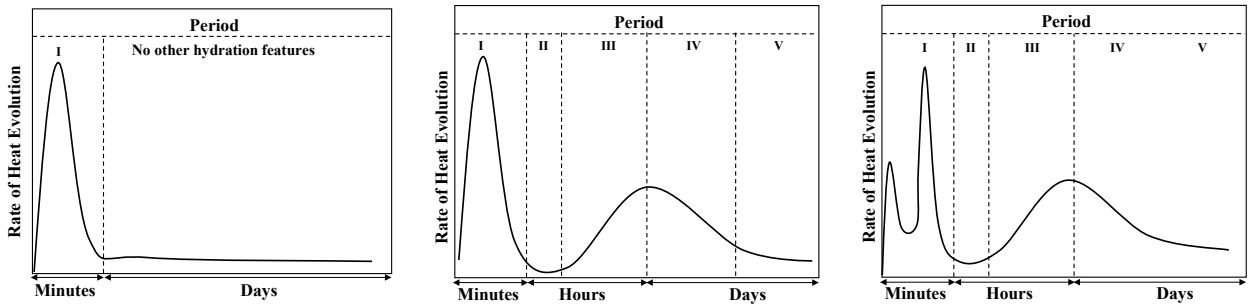

(a) Type 1 (b) Type 2 (c) Type 3

Figure 2. Classification of the exothermic curve of the alkali-activation reaction (I-Initial hydration stage; II-Induction period; III-Acceleration period; IV-Decay period; V-Extended period).

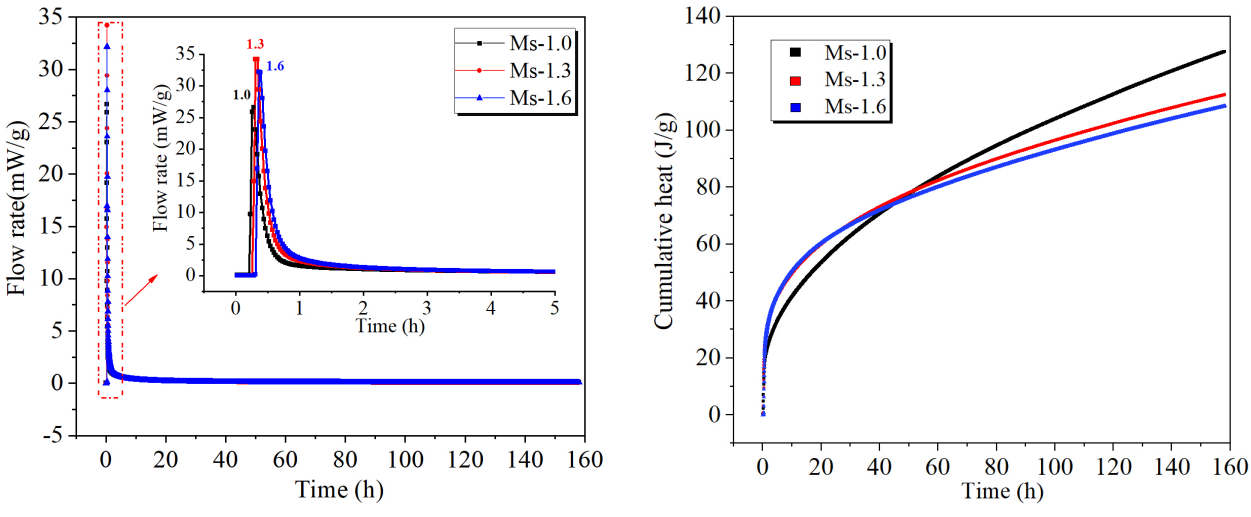

(a) Flow rate (b) Cumulative heat

Figure 3. Exothermic curve of the FA/S system alkali-activation reaction.

Phase composition

The phase composition of FABGC is shown in Figure 4. The primary mineral component of FA and S is the glass phase, with minor quantities of crystalline minerals such as mullite and quartz [30]. However, the FA/S system produces zeolite phase materials after the alkali-activation reaction, indicating that there is a new phase formation during this process, consistent with Li et al.'s findings [29-32].

As depicted in Figure 4, the sodium water glass solution of varying moduli did not impact the types of alkali-activation reaction products in the FA/S system. Quartz, dolomite, calcite, mullite, albite and other zeolite phase substances exist in these three systems. N-A-S-H gel is an amorphous substance. Through the analysis of the High-Score software, the phase in the 30°~40° range of the diffraction spectrum is $NaAlSi_2O_6$, which corresponds to N-A-S-H gel.

The intensity of the quartz characteristic peaks increases with the age, as depicted in Figure 4, indicating the ongoing FA/S dissolution and alkaline-activation reactions. In Ms-1.0, the peak intensities of dolomite and calcite are higher at every age. In Ms-1.3, the characteristic peak intensity of dolomite and calcite increases with the age, indicating that the relative content of these two substances increase with the age. In Ms-1.6, the characteristic peak intensities of dolomite and calcite gradually increase from 3 to 14 d, but they significantly decrease at 28 d.

The variation in the modulus of sodium water glass leads to notable differences in the intensities of the characteristic peaks between dolomite and calcite. At the same age, as the modulus of sodium water glass increases, the characteristic peak intensities of dolomite and calcite in FABGC gradually decrease. This is because, during the alkali-activation reaction, as the modulus of sodium water glass increases, the concentration of OH^- in the solution decreases, and the amount of carbonate (calcite, dolomite, etc.) decreases.

Pore structure characteristics

The cumulative pore volume and pore size distribution curve of FABGC are shown in Figure 5. From Figures 5(a), 5(b), and 5(c), it is evident that the cumulative pore volume of FABGC gradually decreases with the increase in the age. When comparing Ms-1.0 and Ms-1.6 to Ms-1.3, it is clear that the cumulative pore volume of Ms-1.3 is lower at each age. This suggests that a modulus of 1.3 for sodium water glass is more favourable for alkali-activation reactions, enhancing the formation of geopolymer gel [29, 33], and improving the pore structure of FABGC. From Figures 5 (d), (e), and (f), it can be seen that, in Ms-1.0, the maximum pore sizes of FABGC are 650.84 nm, 31.06 nm, 24.18 nm, and 20.95 nm with increasing age and more pores in the range of 500-1000 nm. In Ms-1.3, the maximum pore size of FABGC range from 20 nm to 30 nm, with specific measurements of 29.30 nm, 26.96 nm, 25.12 nm, and 19.60 nm. The maximum pore size ranges for Ms-1.6 and Ms-1.3 are similar, which are 31.08 nm, 28.01 nm, 20.49 nm, and 17.23 nm. The maximum pore size of FABGC decreases with the increasing curing age.

The pores in FABGC can be classified by size as gel pores (< 10 nm), medium capillary pores (10-50 nm), large capillary pores (50-1000 nm), and large pores (> 1000 nm) [34, 35]. The distribution of different pore sizes in FABGC is shown in Figure 6. In general, the volume proportion of gel pores and big pores in FABGC is low, while medium capillary pores and large capillary pores are relatively high. However, the volume ratio of various pores in FABGC prepared by sodium water glass with different modulus is different. In Ms-1.0, the proportion of gel pores in FABGC at different ages was 7-9 %, the proportion of medium capillary pores was 24-42 %, the proportion of large capillary pores was 35-43 %, and the proportion of large pores was 13-26 %. In Ms-1.3, the distribution of pores in each age of FABGC is as follows: gel pores 8-22 %, medium capillary pores 39-52 %, large capillary pores 25-29 %, and large pores 10-18 %. In Ms-1.6, the volume proportions of FABGC

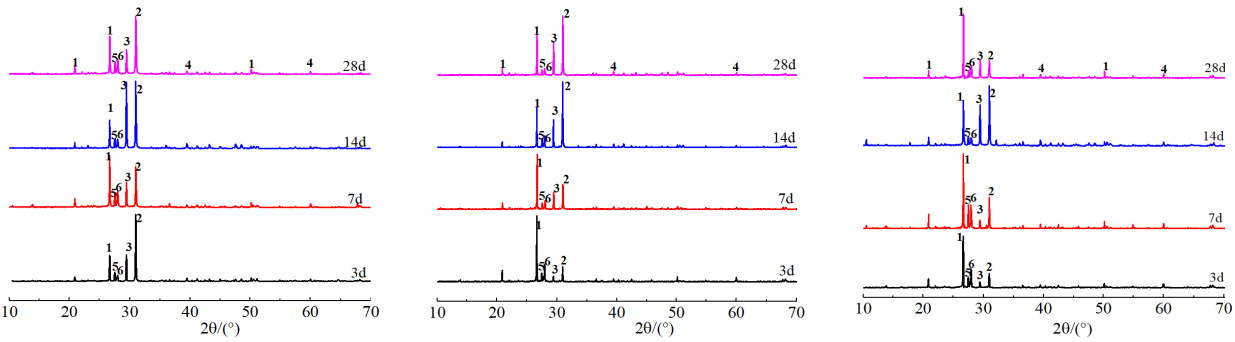

(a) Ms-1.0 (b) Ms-1.3 (c) Ms-1.6

Figure 4. Phase composition of FABGC (1-Quartz; 2-Dolomite; 3-Calcite; 4-Mullite; 5-Zeolite phase; 6-Albite).

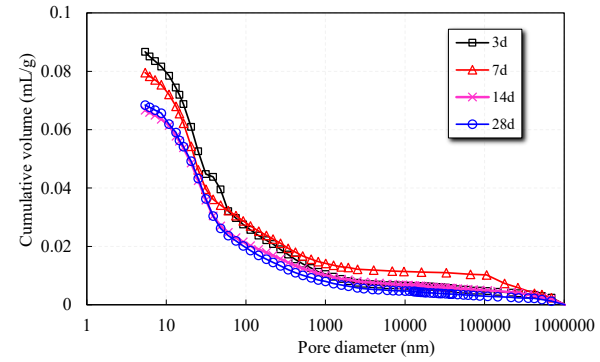

(a) Cumulative pore volume of Ms-1.0

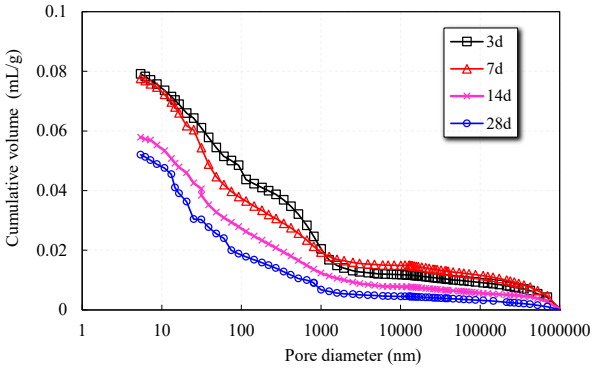

(b) Cumulative pore volume of Ms-1.3

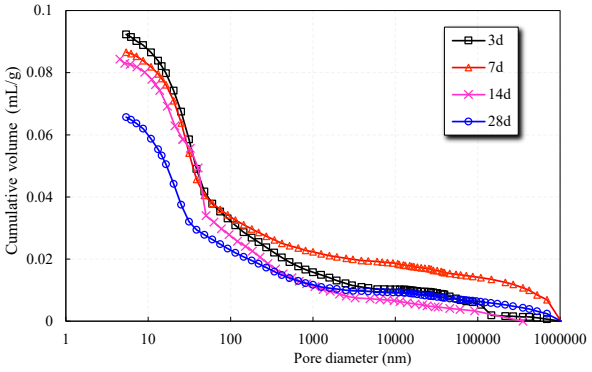

(c) Cumulative pore volume of Ms-1.6

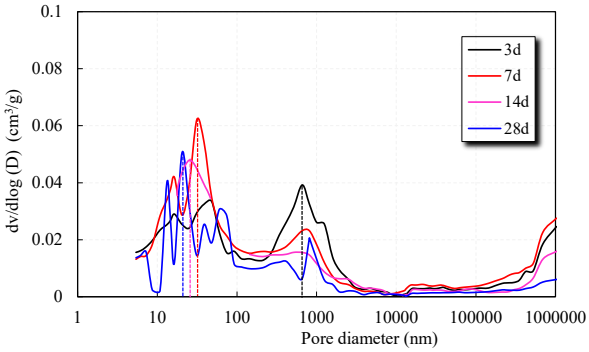

(d) Pore size distribution of Ms-1.0

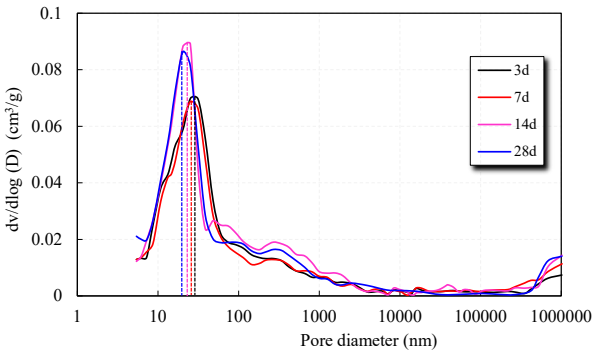

(e) Pore size distribution of Ms-1.3

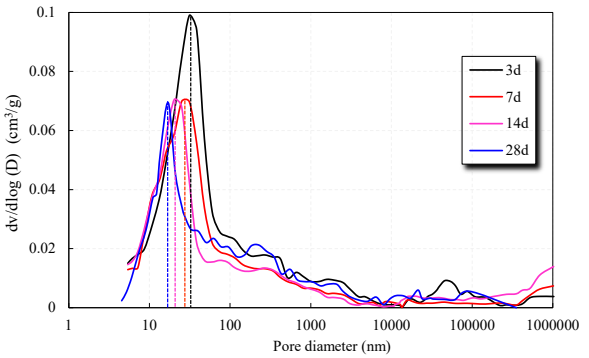

(f) Pore size distribution of Ms-1.6

Figure 5. Cumulative pore volume and pore size distribution curve of the FABGC.

gel pores, medium capillary pores, large capillary pores, and large pores are 5-11 %, 47-55 %, 21-26 %, and 14-26 %, respectively. Through comparison, it is evident that the volume proportion of large capillary pores and large pores in Ms-1.6 are lower compared to Ms-1.0. In Ms-1.3, the internal large pore volume is significantly lower than in Ms-1.6. The proportion of internal gel pore volume is higher in Ms-1.3 than in Ms-1.6 at all the ages, suggesting that an optimal pore structure of FABGC is achieved when the sodium water glass modulus is 1.3. Furthermore, in concrete materials, there are significant differences in the impact of various pore types on the compressive strength. Among them, large pores and large capillary pores are the primary negative factors. Large pores serve as initiation points for cracks, readily causing local stress concentrations and accelerating crack propagation, thereby significantly reducing the compressive strength. Simultaneously, large pores often form permeation pathways, weakening the overall compactness of the material and further decreasing its strength. A high content of large capillary pores also decreases the compactness of the concrete, compromising its mechanical properties.

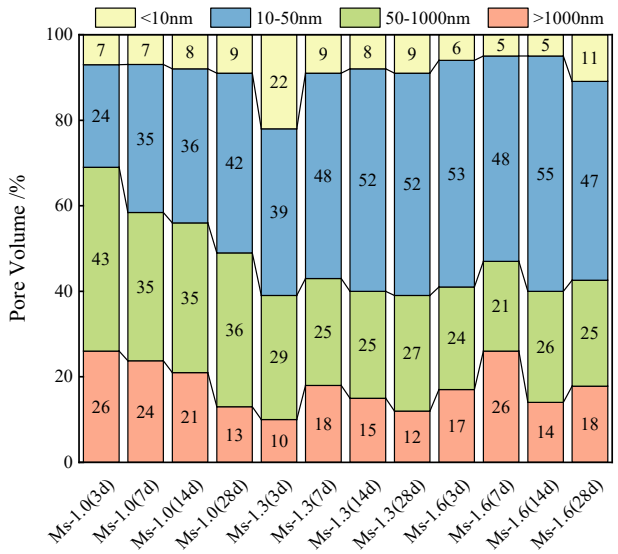

Figure 6. Pore volume fraction of the FABGC.

Microscopic morphology

In the early stage of the alkali-activation reaction, the dissolution rate of the FA/S system under alkaline conditions controls the alkali-activation reaction process. Under identical activity conditions of the cementitious materials, the difference in the micro-morphology of alkali-activated systems prepared with sodium water glass of varying moduli is relatively minor. As the alkali-activation reaction progresses, the FA/S particles continue to dissolve, creating much gel around them. The dissolution rate of FA/S particles varies with the modulus of the alkaline activator, resulting in different microscopic morphology variations in the FABGC produced with varying sodium water glass. When the curing age is 28 d, the microstructure of FABGC is shown in Figure 7. Ms-1.0 has some pores and cracks, but the unreacted FA particles are few, and the dissolution degree of FA is high. In MS-1.3, there are minor cracks and pores, and the overall structure of the matrix is dense. In Ms-1.6, there are many unreacted FA particles, with a lower degree of FA dissolution and more pores and cracks. The overall density of the matrix is poor.

Compared to Ms-1.0, Ms-1.3 shows fewer cracks and better matrix compactness. However, compared to Ms-1.6, Ms-1.3 has fewer unreacted FA particles, indicating that the alkali-activation reaction is more sufficient. When the modulus of sodium water glass is 1.3, it is more conducive to developing the microstructure of the matrix. This is because the concentration of silicate and OH^- in Ms-1.3 is suitable, increasing soluble silicate content in the alkaline activator. This facilitates polymerisation reactions, enhances the dissolution of FA particles, promotes alkaline-activation reactions, and enhances the microstructure of the FABGC matrix.

CONCLUSION

Considering the influence of the modulus of alkali activator on the performance of FABGC, this paper systematically studied the early age compressive strength, alkali activation exothermic characteristics, phase composition, pore structure and microstructure of FABGC prepared by different modulus sodium water glass. The main findings are as follows:

(1) Ms-1.0 and Ms-1.3 exhibit higher compressive strengths, which increase progressively with the age. However, Ms-1.3 is more effective in enhancing the compressive strength development. In contrast, Ms-1.6 exhibits lower compressive strength and develops at a slower rate with the age.

(2) There is no difference in the induction period, acceleration period, decay period, or extended period during the exothermic process of the alkali activated FA/S system, and only one exothermic peak appears in the initial exothermic stage. The lower the modulus of sodium water glass, the higher the total heat release of the alkali-activation reaction, leading to a more complete reaction. In addition, the lower the modulus of sodium water glass, the faster the alkali-activated FA/S system reaches the peak of the alkali-activation reaction rate, but the peak of the alkali-activation reaction rate of Ms-1.3 is the largest.

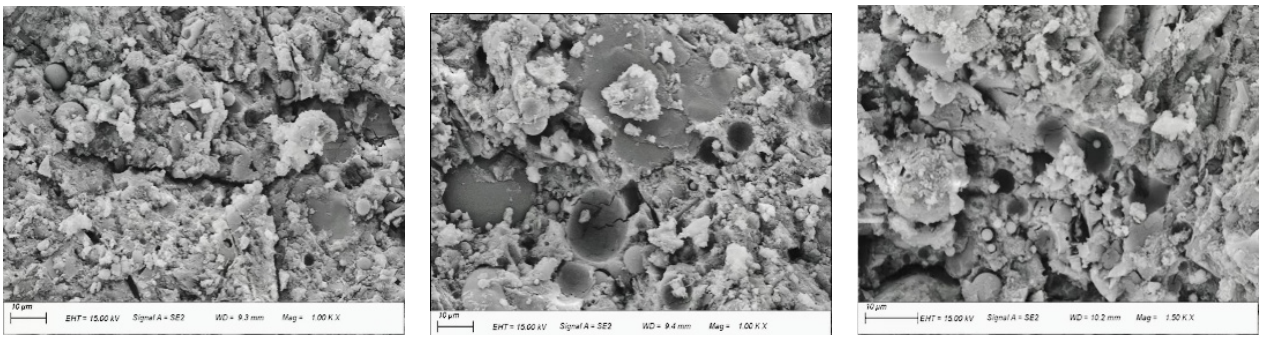

(a) Ms-1.0 (b) Ms-1.3 (c) Ms-1.6

Figure 7. Micromorphology of the FABGC prepared by sodium water glass solution with different moduli.

(3) The FABGC phase contains quartz, dolomite, calcite, mullite, albite, N-A-S-H gel, and other zeolite phase materials. The alkaline concentration is higher in the Ms-1.0 and Ms-1.3 groups, and the amount of carbonate generation increases with the age. However, the amount of carbonate produced in Ms-1.6 initially increases and then decreases with the age.

(4) As the modulus of sodium water glass increases, the cumulative pore volume of FABGC first decreases and then increases, with the maximum pore size concentrated at 10-100 nm, decreasing as the ages increase. In addition, in Ms-1.0, there is a high proportion of gel pores, a low proportion of big pores, and the pore structure is optimal.

(5) There are more cracks in Ms-1.0, while there are more unreacted FA particles in Ms-1.6 and the alkaline-activation reaction is inadequate. In Ms-1.3, there are fewer unreacted FA particles, and the matrix is highly compact.

Acknowledgements

This research was supported by the Natural Science FouThe authors would like to acknowledge the National Natural Science Foundation of China (Grant NO. 52278216), Shaanxi Provincial Natural Science Foundation Project (Project Number: 2023-JC-QN-0631), TianDi Technology Co., Ltd. Technology Innovation and Entrepreneurship Fund Special Project (Project Number: 2023-2-TD-ZD021).

REFERENCES

1. Maddalena R., Roberts J. J., Hamilton A. (2018): Can Portland cement be replaced by low-carbon alternative materials? A study on the thermal properties and carbon emissions of innovative cements. *Journal of cleaner production, 186*, 933-942. Doi: 10.1016/j.jclepro.2018.02.138
2. Truc T. T., Minh H. N., Do Quang, M. (2025): Fly ash-based geopolymer mortars using seawater and sea sand. *Ceramics–Silikáty, 69*(1), 9-18. Doi: 10.13168/cs.2024.0061
3. Cai Y. X., Liu Q. F. (2023): Numerical estimation on chloride erosion resistance of alkali-activated concrete. *J. Build. Mater, 26*(6), 596-603.
4. Zhu H., Zhang Y., Li H. (2023): Effect of Ultra-fine Fly Ash and Superplasticizer on Properties of AlkaliActivated Fly Ash Binder at Room Temperature. *J. Build. Mater, 26*, 419-428.
5. Kucukgoncu H., Özbayrak A. (2024): Microstructural analysis of low-calcium fly ash-based geopolymer concrete with different ratios of activator and binder under high temperatures. *Arabian Journal for Science and Engineering,* 1-27. Doi: 10.1007/s13369-024-09266-1
6. Fu Q., Xu W., Zhao X., Bu M., Yuan Q., Niu D. (2021): The microstructure and durability of fly ash-based geopolymer concrete: A review. *Ceramics International, 47*(21), 29550-29566. Doi: 10.1016/j.ceramint.2021.07.190
7. Hassan A., Arif M., Shariq M. (2020): Mechanical behaviour and microstructural investigation of geopolymer concrete after exposure to elevated temperatures. *Arabian Journal for Science and Engineering, 45*(5), 3843-3861. Doi: 10.1007/s13369-019-04269-9
8. Davidovits J. (2013). Geopolymer cement, A review. Geopolymer Science and Technics, *Technical paper 21*, 1-11.
9. Hadi M. N., Al-Azzawi M., Yu T. (2018): Effects of fly ash characteristics and alkaline activator components on compressive strength of fly ash-based geopolymer mortar. *Construction and Building Materials, 175*, 41-54. Doi: 10.1016/j.conbuildmat.2018.04.092
10. Koushkbaghi M., Alipour P., Tahmouresi B., Mohseni E., Saradar A., Sarker P. K. (2019): Influence of different monomer ratios and recycled concrete aggregate on mechanical properties and durability of geopolymer concretes. *Construction and Building Materials, 205*, 519-528. Doi: 10.1016/j.conbuildmat.2019.01.174
11. Wianglor K., Sinthupinyo S., Piyaworapaiboon M., Chaipanich A. (2017): Effect of alkali-activated metakaolin cement on compressive strength of mortars. *Applied Clay Science, 141*, 272-279. Doi: 10.1016/j.clay.2017.01.025
12. De Azevedo A. R., Teixeira Marvila M., Barbosa de Oliveira L., Macario Ferreira W., Colorado H., Rainho Teixeira S., Mauricio Fontes Vieira C. (2021): Circular economy and durability in geopolymers ceramics pieces obtained from glass polishing waste. *International Journal of Applied Ceramic Technology, 18*(6), 1891-1900. Doi: 10.1111/ijac.13780
13. Zhang J., Shi C., Zhang Z., Ou Z. (2017): Durability of alkali-activated materials in aggressive environments: A review on recent studies. *Construction and Building Materials, 152*, 598-613. Doi: 10.1016/j.conbuildmat.2017.07.027
14. Lee W. K. W., Van Deventer J. S. J. (2002): The effects of inorganic salt contamination on the strength and durability of geopolymers. *Colloids and Surfaces A: Physicochemical and Engineering Aspects, 211*(2-3), 115-126. Doi: 10.1016/S0927-7757(02)00239-X
15. Hu Z. (2013). Early hydration and shrinkage of alkali-activated slag/fly ash blend cement. *Hunan University.*
16. Mao M.J., Ren J.Y., Zhang W.B., Chen W. (2016): Study on the mechanical properties of fly ash geopolymer concrete. *Concrete, 5,* 78-80.
17. Cao W.W., Lei T., Min Z.H., Xu X.L., Duan P.P. (2021): Performance and mechanism of solid alkali-activated slag / fly ash grouting material. *Bull Chin Ceram Soc, 40*(12),4037-4043.
18. Cho Y. K., Yoo S. W., Jung S. H., Lee K. M., Kwon S. J. (2017): Effect of Na_2O content, SiO2/Na_2O molar ratio, and curing conditions on the compressive strength of FA-based geopolymer. *Construction and Building Materials, 145*, 253-260. Doi: 10.1016/j.conbuildmat.2017.04.004
19. Huseien G. F., Mirza J., Ismail M., Hussin M. W. (2016): Influence of different curing temperatures and alkali activators on properties of GBFS geopolymer mortars containing fly ash and palm-oil fuel ash. *Construction and Building Materials, 125,* 1229-1240. Doi: 10.1016/j.conbuildmat.2016.08.153
20. Phoo-ngernkham T., Chindaprasirt P., Sata V., Hanjitsuwan S., Hatanaka S. (2014): The effect of adding nano-SiO_2 and nano-Al_2O_3 on properties of high calcium fly ash geopolymer cured at ambient temperature. *Materials & Design, 55,* 58-65. Doi: 10.1016/j.matdes.2013.09.049
21. Ismail I., Bernal S. A., Provis J. L., San Nicolas R.,

Hamdan S., van Deventer J. S. (2014): Modification of phase evolution in alkali-activated blast furnace slag by the incorporation of fly ash. *Cement and Concrete Composites, 45*, 125-135. Doi: 10.1016/j.cemconcomp.2013.09.006

22. Chen Y.L., Zeng H., Li T.Y., Liu Z.F. (2021): Development and Application of Metakaolin, Fly Ash and Slag Geopolymer Grouting Material. *Highw Eng, 46*(06), 142-147.
23. Li Z.M. (2019). *Study on cementitious material and concrete performance of slag/fly ash base polymer.* Shenyang, Shenyang Jianzhu University.
24. Li R.W. (2020). *Study on mechanical properties and freezing resistance of fly ash geopolymer concrete.* Yinchuan, Ningxia University.
25. CABP (China Architecture & Building Press) (2003). GB/T50081-2002: Standard for test method of mechanical properties on ordinary concrete. CABP, Beijing, China.
26. Muller A. C. A., Scrivener K. L. (2017): A reassessment of mercury intrusion porosimetry by comparison with 1H NMR relaxometry. *Cement and Concrete Research, 100,* 350-360. Doi: 10.1016/j.cemconres.2017.05.024
27. Ridtirud C., Chindaprasirt P., Pimraksa K. (2011): Factors affecting the shrinkage of fly ash geopolymers. *International Journal of Minerals, Metallurgy, and Materials, 18*(1), 100-104. Doi: 10.1007/s12613-011-0407-z
28. Shi C., Day R. L. (1995): A calorimetric study of early hydration of alkali-slag cements. *Cement and Concrete Research, 25*(6), 1333-1346. Doi: 10.1016/0008-8846(95)00126-W
29. Fernández-Jiménez A., Palomo Á., Sobrados I., Sanz J. (2006): The role played by the reactive alumina content in the alkaline activation of fly ashes. *Microporous and Mesoporous materials, 91*(1-3), 111-119. Doi: 10.1016/j.micromeso.2005.11.015
30. Li H., Zhuge L., Shi S., Xu D. (2012): Hydration products of fly ash based cementing material activated by NaOH. *Journal of the Chinese Ceramic Society, 40*(2), 234-239.
31. Ng C., Alengaram U. J., Wong L. S., Mo K. H., Jumaat M. Z., Ramesh S. (2018): A review on microstructural study and compressive strength of geopolymer mortar, paste and concrete. *Construction and Building Materials, 186,* 550-576. Doi: 10.1016/j.conbuildmat.2018.07.075
32. Fernández-Jiménez A., Palomo A. (2005): Composition and microstructure of alkali activated fly ash binder: Effect of the activator. *Cement and concrete research, 35*(10), 1984-1992. Doi: 10.1016/j.cemconres.2005.03.003
33. Huanhai, Z., Xuequan, W., Zhongzi, X., & Mingshu, T. (1993). Kinetic study on hydration of alkali-activated slag. *Cement and Concrete Research, 23*(6), 1253-1258. Doi: 10.1016/0008-8846(93)90062-E
34. Neubauer C. M. (1997). *On the chemistry, microstructure, and deformation properties of cement pastes: towards a new strategy for controlling drying shrinkage.* Northwestern University.
35. Wang Q., Li S., Pan S., Cui X., Corr D. J., Shah S. P. (2019): Effect of graphene oxide on the hydration and microstructure of fly ash-cement system. *Construction and Building Materials, 198*, 106-119. Doi: 10.1016/j.conbuildmat.2018.11.199